

Slice-and-Forge: Making Better Use of Caches for Graph Convolutional Network Accelerators

Mingi Yoo*
Yonsei University
Seoul, South Korea
skys7297@yonsei.ac.kr

Jaeyong Song*
Yonsei University
Seoul, South Korea
jaeyong.song@yonsei.ac.kr

Hyeyoon Lee
Yonsei University
Seoul, South Korea
hylee817@yonsei.ac.kr

Jounghoo Lee
Yonsei University
Seoul, South Korea
jounghoolee@yonsei.ac.kr

Namhyung Kim
Samsung Electronics
Hwaseong, South Korea
namhyungk11@gmail.com

Youngsok Kim
Yonsei University
Seoul, South Korea
youngsok@yonsei.ac.kr

Jinho Lee[†]
Seoul National University
Seoul, South Korea
leejinho@snu.ac.kr

ABSTRACT

Graph convolutional networks (GCNs) are becoming increasingly popular as they can process a wide variety of data formats that prior deep neural networks cannot easily support. One key challenge in designing hardware accelerators for GCNs is the vast size and randomness in their data access patterns which greatly reduces the effectiveness of the limited on-chip cache. Aimed at improving the effectiveness of the cache by mitigating the irregular data accesses, prior studies often employ the vertex tiling techniques used in traditional graph processing applications. While being effective at enhancing the cache efficiency, those approaches are often sensitive to the tiling configurations where the optimal setting heavily depends on target input datasets. Furthermore, the existing solutions require manual tuning through trial-and-error or rely on sub-optimal analytical models.

In this paper, we propose *Slice-and-Forge* (SnF), an efficient hardware accelerator for GCNs which greatly improves the effectiveness of the limited on-chip cache. SnF chooses a tiling strategy named feature slicing that splits the features into vertical slices and processes them in the outermost loop of the execution. This particular choice results in a repetition of the identical computational patterns over irregular graph data over multiple rounds. Taking advantage of such repetitions, SnF dynamically tunes its tile size. Our experimental results reveal that SnF can achieve 1.73× higher performance in geomean compared to prior work on multi-engine settings, and 1.46× higher performance in geomean on small scale settings, without the need for off-line analyses.

CCS CONCEPTS

• **Computer systems organization** → **Neural networks; Single instruction, multiple data.**

KEYWORDS

Graph Convolutional Networks, Accelerators, Caches

1 INTRODUCTION

Graph convolutional networks (GCNs) are considered the next-generation deep neural networks (DNNs) as they can be applied to a variety of data which exhibit irregular patterns. Despite their wide applicability spanning from traditional graph problems [16, 81] to modern DNN tasks [70], conventional DNN accelerators cannot efficiently accelerate GCNs. Different from traditional DNNs, graphs exhibit highly sparse structures and demand fundamentally different acceleration schemes. Although some hardware accelerators which exploit the sparsity in DNNs [35, 54, 83] may cope with the highly sparse structures of graphs, such accelerators are still not well-suited for GCNs as the portion of non-zero values in graphs (<0.01%) is significantly lower than sparse DNNs (10%–90%).

Aimed at the efficient acceleration of GCNs, prior studies propose new hardware accelerators which exploit various unique characteristics of GCNs. In particular, as GCNs incur large working set sizes and highly irregular memory access patterns, the hardware accelerators should efficiently utilize their limited on-chip caches. Viewing GCNs as cascaded sparse-dense matrix multiplications, one popular technique is loop tiling and reordering, as demonstrated in [17, 46, 50]. Loop tiling partitions a given GCN into multiple tiles, as performed in sparse matrix-vector multiplication (SpMV) approaches [26, 89]. By confining the working set to a specific region, the loop tiling result in better cache efficiency at the expense of increased repetition counts.

However, the difficulty of loop tiling lies in the fact that configuring the tile size is non-trivial. Especially for GCNs which exhibit abundant random accesses, the optimal setting for tiling varies per dataset and cannot be decided statically. Thus, the current existing solution to obtain the optimal tiling configuration is manual tuning through trial-and-error. While there exists an approach to restrictively apply analytical search for tiling configuration [46], it ignores the fact that the graph is sparse and often falls into an inferior solution.

This is an author preprint version of a paper which will appear in the proceedings of PACT’22.

* Equal contribution

[†] Corresponding author.

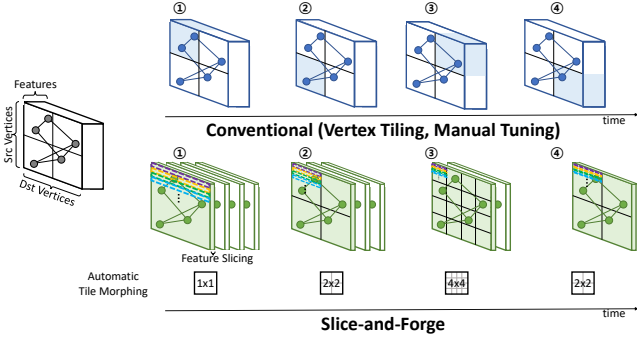


Figure 1: Conceptual diagram of the slice-and-forge scheme.

In this work, we propose *Slice-and-Forge (SnF)*, a technique for enabling on-line tuning for the GCN configuration. The proposed scheme is conceptually illustrated in Figure 1. SnF sits on top of *feature slicing*, which splits the feature matrix into multiple vertical strips and puts its loop at the outermost level. This creates a repeated access pattern over the random graphs and allows for gradually tuning the configurations such that it can settle at a near-optimal configuration within a few rounds.

Exploiting the repetitive patterns, we propose a method for efficiently tuning the vertex tiling configurations with *automatic tile morphing*. In vertex tiling, the adjacency matrix is partitioned into multiple tiles where the performance is sensitive to tile size. With automatic tile morphing, we search for the optimal tile size using a method similar to a convex optimization.

Although the feature slicing itself is a kind of loop tiling technique that has been long studied in the context of SpMM [2, 86] or GCNs [46], exploiting the repetitive pattern from feature slicing for dynamic configuration has not been studied yet, to the best of our knowledge. In addition to enabling the repetitive dynamic configuration, we also show that feature slicing itself is often a favorable choice for loop tiling.

Our contributions can be summarized as follows:

- We identify that feature slicing creates repetitive patterns over a random graph data and propose Slice-and-Forge (SnF) which exploits the pattern for efficient dynamic tuning.
- We suggest automatic tile morphing that dynamically tunes the number of vertex tiles at runtime.
- We provide a strategy for extending SnF to multi-chip module scaling.
- We provide a thorough evaluation of SnF which composes the above techniques, and we discuss the benefits.

2 BACKGROUND

2.1 Graph Convolutional Networks

With numerous variations [23, 39, 74], inference of a GCN layer l can be formulated as follows:

$$X^{(l+1)} = \sigma(\tilde{A} \cdot X^{(l)} \cdot W^{(l)}). \quad (1)$$

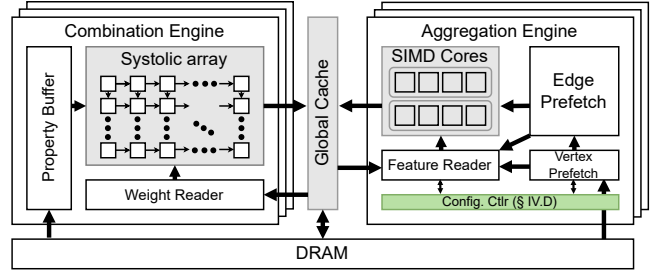


Figure 2: Baseline GCN accelerator architecture.

In the above equation, $\tilde{A} \in \mathbb{R}^{|V| \times |V|}$ is a normalized Laplacian¹. $X^{(l)} \in \mathbb{R}^{|V| \times |F^{(l)}|}$ is a feature matrix for the l -th layer where each row represents the features associated with a vertex. $W^{(l)} \in \mathbb{R}^{|F^{(l)}| \times |F^{(l+1)}|}$ is a trainable weight matrix for layer l and is the trainable part of GCNs. $\sigma(\cdot)$ is an activation function where the rectified linear unit (ReLU) is commonly used. Typically, three to five layers comprise a GCN [44, 48] as having too many layers is known to be difficult to train.

Eq. (1) has two matrix multiplications in it. The first, matrix multiplication between \tilde{A} and $X^{(l)}$ or \tilde{A} and $X^{(l)} \cdot W^{(l)}$, is called the *aggregation* phase. Because each row of \tilde{A} represents the neighbor list of a vertex, multiplying the row with matrix $X^{(l)}$ essentially ‘aggregate’s features of neighboring vertices. While summation is the most popular aggregation function, many aggregation functions other than summation is possible (e.g., max). Nonetheless, the underlying computation pattern is identical to matrix multiplication. The second, matrix multiplication between $\tilde{A} \cdot X^{(l)}$ and W or $X^{(l)}$ and W , is called the *combination* phase. Because the elements within an entire row represents features belonging to a single vertex, the multiplication does not incur any information transfer between the vertices, but just ‘combine’s the features contained within the vertex. In other words, it does not require inter-vertex communication. To each vertex, it can be thought as the feature vector being passed through a fully connected layer, where each vertex shares an identical weight matrix.

As analyzed in [75], aggregation phase usually becomes the main bottleneck of the GCN execution. Unlike the combination which is essentially a dense-dense matrix multiplication, the high sparsity of the graph topology (\tilde{A}) and the low arithmetic density of the aggregation phase yields an extremely memory-intensive characteristics. Together with the reason that it is hard to optimize, many work mainly focus on the aggregation phase. It is also worth noting that as depicted in Eq. (1), the order between aggregation and combination does not affect the result of a GCN layer. However, depending on the shape of W , the width of the feature vector could increase or decrease, which can be used to reduce the execution time of aggregation [45].

2.2 Baseline GCN Accelerator

Figure 2 presents a baseline GCN accelerator comprising aggregation engines and combination engines, similar to previous work [8,

¹Normalized Laplacian refers to a form of adjacency matrix defined as $\tilde{A} = I - D^{-1/2}AD^{-1/2}$ where D is a degree matrix.

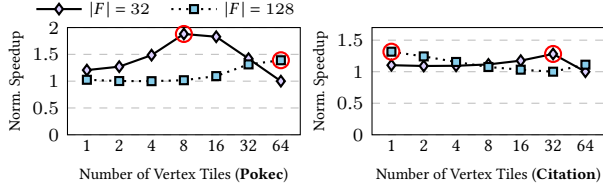


Figure 3: Sensitivity of GCN to number of vertex tiles. The best performing number of vertex tiles are marked with red circles.

38, 50, 75], where the green component has been newly added that will be discussed in Section 4.3. The core of combination engine is a systolic array to support efficient matrix multiplication. Similar to previous systolic array based DNN accelerators [34, 51], there are two local memories in a double buffering manner that continuously provide input to the core. The property buffer X , and the weight reader provide W , respectively. The output of the combination engine is read by the aggregation engine such that it can be processed in the aggregation function.

The aggregation phase is similar to classic graph processing, but each access to the edge contains a wide row of X that has to be multiplied to the corresponding edge weight (i.e., $\tilde{A}_{i,j}$) and accumulated. The SIMD cores process the multiply-accumulation. To feed the SIMD cores without stall, the two prefetch modules runs ahead in the graph topology such that the feature reader can always have on-the-fly reads to the feature matrix X .

The graph topology is stored in a compressed sparse row (CSR) format to exploit the sparsity of the data. The vertex prefetch unit reads row pointers and passes it to edge prefetch and feature reader. Then the edge prefetch unit reads column indices of CSR and sends them to the feature reader and SIMD cores. When the feature reader receives an edge, it collects the rows of the feature matrix X . Because edges are sparse, the reads exhibit highly randomized pattern, making the aggregation phase memory-intensive and hard to optimize.

One way to mitigate the memory bottleneck in the aggregation phase is to use a large on-chip global cache. Shared by multiple engines in the accelerator, it temporarily stores the recently accessed features. However, because of the wide feature matrix whose width often spans over hundreds to thousands, the working set usually well exceeds the size of the global cache, making it difficult to exploit localities.

3 MOTIVATIONAL EXAMPLE

In GCN execution, the most commonly used loop tiling technique to reduce memory accesses is *vertex tiling* as adopted from [17, 46, 50]. With vertex tiling, the adjacency matrix is split into multiple tiles and processed sequentially. This way, the range of features being accessed is restricted within a tile to have a much smaller cache working set (and therefore exhibit more cache hits). However, a better cache hit ratio incurs at the expense of multiple accesses on vertex features, either for reading or writing the features. Because of this, choosing the right number of tiles becomes critical for high performance.

Figure 3 illustrates sensitivity to the number of vertex tiles, according to graph datasets Pokec and Citation (See Table 1 for details.) with different feature width per vertex (32 and 128). The Y axis shows speedup, normalized by the slowest among the number of tiles under consideration.

We make two observations from the plots: the performance is sensitive to the number of tiles, and the optimal number of vertex tiles differs according to dataset and feature width. With the default 1×1 vertex tiles, much of the memory access count is spent reading the vertex features multiple times due to cache misses. As the number of tiles increases, the working set size decreases and is better captured by the cache. Simultaneously, the number of output feature access increases due to the repeated writes². It is shown that the performance discrepancy between the best and the worst configuration greatly varies, up to $1.9\times$ in the example (Pokec at $|F| = 32$). Furthermore, the relation between the amount of input access and number of tiles depends on the random access pattern posed by the adjacency matrix. Not knowing the optimal setting a priori, one has to make an educated guess that can easily result in an inferior performance, or undergo several executions to find the optimal configuration which destroys the purpose of achieving speedup.

In this paper, we suggest feature slicing as an opportunity for on-line tiling configuration. By exploiting the repetitive computation pattern found from feature slicing dataflow, the optimal configuration is gradually found over multiple rounds. The proposed scheme not only searches for the optimal vertex tiling, but also the work distribution strategy which is crucial for multi-engine scaling of the GCN accelerators.

4 SLICE-AND-FORGE

4.1 Feature Slicing Dataflow

Much of the prior work on GCN accelerations are based either on the *row product* [8, 46, 50, 75] or *column product* [17]. In this section, we describe the dataflow choice of SnF, which places feature slicing as the outermost loop that embraces vertex tiling.

Figure 4 (left) displays the aggregation based on the basic row product dataflow (the innermost loop outputs a row). The colored strips of \tilde{A} represent nonzeros in the topology matrix (i.e., edges) and the horizontal strips of X are the elements of the feature vectors to be aggregated from the matching colored edges. In the row product execution model, ① the outermost loop visits the vertices in \tilde{A} . ② The next level loop visits the edges and ③ aggregates the corresponding features.

The memory access pattern from this dataflow exhibits the following characteristics: First, reading \tilde{A} is done sequentially and only once. Second, features from neighboring vertices are read randomly over the entire feature matrix $X^{(l)}$, where a row of the feature matrix is read for each of the edges in \tilde{A} . Lastly, writing the output feature $X^{(l+1)}$ to the memory is also sequential and performed only once. From the above characteristics, the performance bottleneck is at reading the feature matrix $X^{(l)}$. With a global cache, the memory access can be reduced if the cache is large enough to capture the features, where the hit rate depends on the pattern of the edges.

²In fact, it is possible to alter the order of tile traversal to increase the input access repetition instead. We omit this case as it mandates perfect caching.

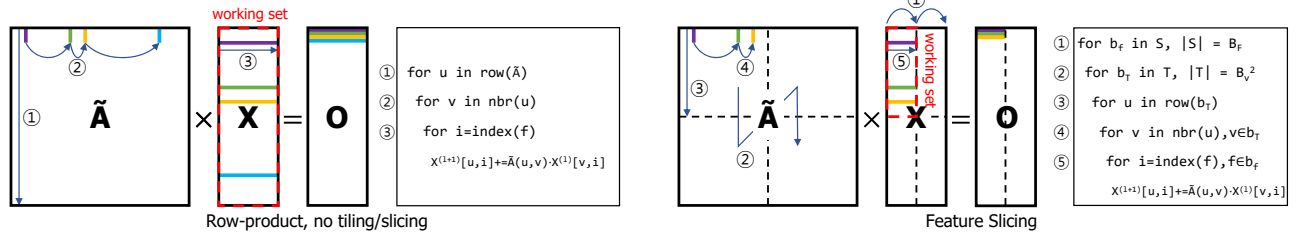


Figure 4: Row product based GCN processing (left) and feature slicing (right).

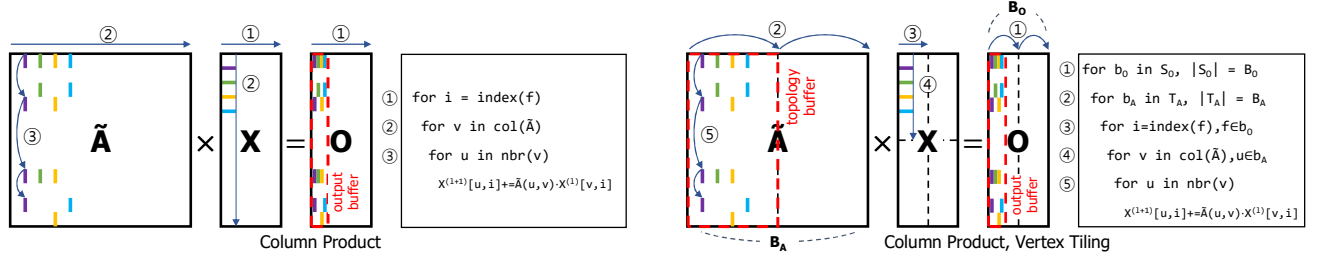


Figure 5: Column product based execution (left) and its tiling (right).

When the feature matrix is significantly larger than the global cache size, the miss rate approaches 100% and loop tiling is a popular solution for mitigating this. While there are many possible configurations, Figure 4 (right) shows the choice of SnF named *feature slicing*. It partitions \tilde{A} into $B_V \times B_V$ vertex tiles, and splits the feature matrix X into multiple *slices* of vertical strips. As depicted in the figure, the two outermost loops (① and ②) visit the feature slices and vertex tiles. The inner loops are identical to that from the Figure 4 (left). As observed in the dotted red lines, the working set is divided by the number of feature slices B_F and number of tiles B_V , at the expense of reading the topology \tilde{A} for B_F times and reading the feature matrix X for B_V times.

When B_V and B_F are large enough that all the tiles perfectly fit on the on-chip memory, only the cold misses remain. In this manuscript, we call this strategy *perfect tiling*. While perfect tiling can maximize the cache efficiency, the required value of B_V is usually too large. Moreover, it neglects the sparsity of the graph topology and regards the computation as a dense matrix multiplication, often resulting in a suboptimal performance.

Column product is another dataflow solution for mitigating the cache miss. Figure 5 (left) shows the column product execution model. ① The outermost loop traverses each element along the feature vectors (i.e., the column of X). ② The next level loop visits the columns of \tilde{A} . ③ Lastly, the nonzero elements in the chosen column of \tilde{A} are accessed, and the multiplied value is written to the corresponding position of the output matrix.

Because the two dimensions of X are located at the outer loop, X is accessed only once. However, it requires access to the adjacency matrix by the length of feature. For mitigating this, there is a way that use cache for adjacency matrix like Figure 5 (right). When \tilde{A} and O are split into B_A and B_O vertical strips, respectively, a strip of \tilde{A} stored in the cache is reused multiple times to improve

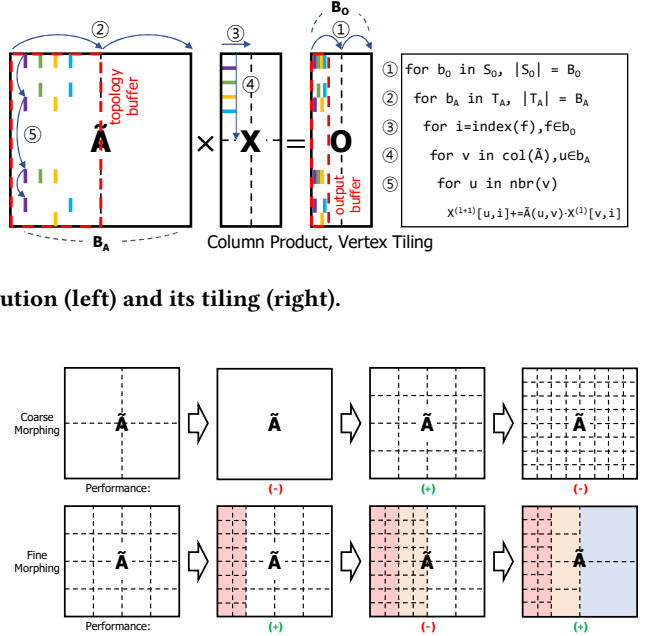


Figure 6: Procedure of automatic tile morphing.

performance, but it needs an extra cache capacity and adds the cost of repeated access to the output matrix.

In SnF, we place the feature slice visiting loop at the outermost level (①). Even though the order of the two loops does not pose much difference in the working set size except for slight change in the pattern, it should be emphasized that this particular choice creates a recurring pattern over the random data access ②–⑤. This creates a unique opportunity for GCNs, where the inner loop configuration can be tuned over iterations of the loop ① because there is no difference among the feature slices, unlike the vertex tiles. Please note that this technique is infeasible for classic graph analytics, because the feature width is usually too narrow (e.g., 1 for PageRank).

The size of B_F has to be decided such that the slice width $|F|/B_F$ must be at least over 64 B, which is the granularity of the main memory and cache lines to maintain the spatial locality. SnF sets the slice width to be 64 bytes (e.g., $B_F = 16$ for $|F| = 256$).

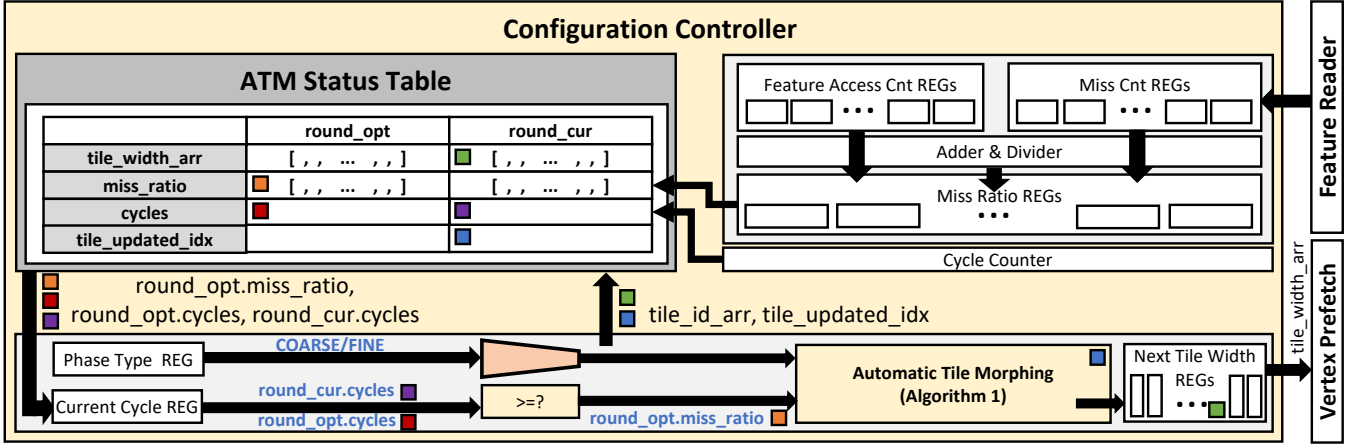


Figure 7: Configuration controller architecture to support automatic tile morphing.

4.2 Automatic Tile Morphing

As exemplified in Section 3, choosing the right number of tiles is crucial to achieving high performance, yet there is no efficient method for optimal selection without an expensive trial-and-error procedure. We propose *automatic tile morphing*, an approach that takes advantage of repetitive computational patterns to gradually configure the vertex tiling at runtime.

With feature slicing dataflow (Section 4.1, the topology data \tilde{A} is traversed multiple (B_F) times in the exact same pattern (②-⑤ in Figure 4 (right)). From each round—processing a slice of X —of the execution, automatic tile morphing dynamically tunes the vertex tiling to reach the nearly optimal point at runtime, without the need for off-line design space exploration. While a similar dynamic method can be devised by executing vertex tiling as outer loop and tuning $|F|$ as the parameter, the processing pattern of each tile would be distinct, making the tuning result from one tile unusable to the next.

Figure 6 displays an example procedure of automatic tile morphing, comprising two phases: *coarse morphing* and *fine morphing*. Coarse morphing (top) assumes that performance is a convex function of the number of tiles. Starting from a default setting (2×2 in the figure), the performance is measured with twice more tiles in each dimension, and then half the number of tiles in each dimension. In the direction of better performance, the same doubling or merging continues until a decrease in the performance is observed, the number of tiles is rolled back to that of the previous iteration (4×4 in the example), and the coarse morphing terminates.

Then, fine morphing (bottom) starts from the best partitioning of the coarse morphing phase. The goal of fine morphing is to use heterogeneously sized tiles, such that the unbalanced graph distribution is considered. Real-world graphs are sometimes collected by crawling, which is based on a breadth-first search order. In addition, because of the small-world phenomenon [41], dense clusters often exist. These clusters exhibit a larger number of access instances and likely require a smaller working set compared to the sparser region of the graph. We confined the tiling to have variable-sized vertical

strips of square tiles to reduce the search space size, which effectively converts fine morphing to a one-dimensional partitioning problem.

Fine morphing records the hit rates of each tile and uses the rates to determine the visiting order. In the order of the lowest hit rate (red \rightarrow orange), the vertical strips of blocks are further split into half-sized tiles, with one column per iteration. Similar to coarse morphing, this process is performed until performance degrades, and it rolls back the change that degraded the performance. Then, similarly, but in the order of the highest hit rate (blue), two adjacent columns are merged until the performance decreases. While we can further examine splitting a tile to 4×4 tiles or merging 4×4 tiles into one, we found no case in our dataset where such a configuration could further accelerate the execution.

For implementation, we defined a unit tile size and stored the length of each vertical strip in the units. In practice, the unit tile can be set as the tile size that perfectly fits the global cache. In this paper, we split the topology into 64×64 unit tiles. In the worst case, there can be at most 64 unit-width strips, where storing them consumes less than a KB of capacity.

Empirically, automatic tile morphing finds a solution near the static best. To avoid the decision process from being on the critical path, we decide the next iteration’s policy based on the measurements until the penultimate column of blocks. However, a runtime overhead exists from the few first feature slices being executed with suboptimal tiling. When B_F is too small, the portion of this overhead grows relatively large, which is another reason to favor a higher B_F . Please see Section 6.12 for further discussion.

4.3 Slice-and-Forge Architecture

To support automatic tile morphing, SnF adds a hardware component named *configuration controller* to the accelerator shown in Figure 2. The detailed architecture of the controller is illustrated in Figure 7.

The job of the configuration controller overall is to collect statistics given from the feature reader, make configuration decisions, and pass the decision to the vertex prefetch unit. For each iteration

round of B_F , the controller accumulates the number of feature accesses and misses per vertical strip of unit tiles to calculate miss ratio. When the round is over, the controller updates these miss ratios and cycles into the *ATM Status Table*. Based on this information from current round (*round_cur*) and from the stored optimal (*round_opt*), the controller invokes Algorithm 1 to produce next round's decision for the vertex tile size.

Algorithm 1 Automatic Tile Morphing

```

Input:
  round_cur, round_opt: configuration of current/optimal round
  atm_direction: current ATM morphing direction flag (HALVING/MERGING)
  phase: current ATM phase flag (COARSE/FINE)
Output:
  new_tile_width_arr: next tile width array decided by ATM
1: if round_cur.cycles < round_opt.cycles then // if faster, update to optimal setting
2:   round_opt ← round_cur
3: else if phase = COARSE then // if slower, enter fine morphing
4:   phase ← FINE
5: else // for rest, this setting is optimal we found.
6:   return round_opt.tile_width_arr
7: if phase = COARSE then
8:   if atm_direction = HALVING then // increase the number of the tiles.
9:     for all tiles of round_cur.tile_width_arr do
10:      append halved tiles to new_tile_width_arr. // e.g. [4,4] → [2,2,2,2]
11:   else if atm_direction = MERGING then // decrease the number of the tiles.
12:     for half of tiles in round_cur.tile_width_arr do
13:      append merged tile to new_tile_width_arr. // e.g. [2,2,2,2] → [4,4]
14: else if phase = FINE then
15:   if atm_direction = HALVING then // increase the number of the tiles.
16:     find worst miss ratio tile and halve.
17:     append halved tiles and other tiles to new_tile_width_arr.
18:   else if atm_direction = MERGING then // decrease the number of the tiles.
19:     find best miss ratio tile and merge with adjacent tile.
20:     append merged tile and other tiles to new_tile_width_arr.
21:   round_cur.tile_updated_idx ← index
22:   round_cur.tile_width_arr ← new_tile_width_arr
23: return new_tile_width_arr

```

Algorithm 1 shows the simplified procedure of automatic tile morphing. The controller manages tiling by *tile_width_arr*, an array that stores how many unit tiles comprise each vertical strip. For example, it stores 32 consecutive 2's to represent 32×32 tiles and 16 consecutive 4's to represent 16×16 tiles. Automatic tile morphing starts with updating the optimal value (*round_opt*) in the status table (line 2). The controller proceeds into the *coarse morphing* phase. Assuming that the performance-improving direction *atm_direction* have been found in the previous rounds to be halving the tile sizes (omitted in the algorithm), the new *tile_width_arr* is populated with twice the original elements from the array of the current rounds of half the values (line 8-10). The merging direction functions in a similar manner (line 11-13). In *fine morphing* phase, controller finds the target tile (*t_id*) that should be merged with adjacent tile or halved based on the miss-ratio (line 14-21). After *tile_width_arr* is determined, this tiling information is passed to vertex prefetch unit.

The configuration controller stores access/miss/ratio registers for each of the 64 unit vertical columns. In addition, *tile_width_arr* and *miss_ratio* of the status table are 64 entry-long arrays for each of *round_opt*, *round_cur*, and at the output to the vertex prefetch. Thus, using 4 byte elements, the total size of the registers and status table is only about 1.5KB, a negligible size compared to the global cache.

4.4 Dataflow Cost Comparison

The feature slicing dataflow adopted in SnF implicitly prioritizes increasing the number of slices B_F over increasing the vertex tiles B_V . While it is true that this choice somewhat puts a restriction on loop tiling, we analyze the cost model to show that prioritizing is an advantageous strategy in general.

Using the terms Section 2.1 and $|E|$ as the number of edges, the memory access cost from the row product execution in Figure 4 (left) can be modeled as below.

$$M_{Row} = (|V| + |E|) + m(|V||F|) \cdot |E||F| + |V||F|. \quad (2)$$

The first and third terms account for sequentially reading the topology data in CSR format and writing the output matrix, respectively. The second term, on the other hand, models the random reads to the feature matrix. For each edge ($|E|$) in the topology, a row of the feature matrix is read ($|F|$). Under the assumption that the miss rate $m(x)$ is a function of the working set size x , the second term represents the accesses filtered by the global cache.

Applying loop tiling, the bottleneck at the second term is reduced by reducing the working set size. Using the tiling from Figure 4 (left), the model becomes:

$$M_{FS} = B_F(B_V|V| + |E|) + m\left(\frac{|V||F|}{B_FB_V}\right) \cdot |E||F| + B_V|V||F|. \quad (3)$$

The working set size is divided by the product of $|B_F|$ and $|B_V|$, where those factor are multiplied to reading the topology data and writing the output matrix, accounting for the repetitions.

Thus, intuitively, increasing $|B_F|$ yields a lower cost if the topology data are smaller, and increasing $|B_V|$ is better if the feature matrix size is smaller. Because the feature width in GCNs usually reach several hundreds, it is often beneficial to favor increasing $|B_F|$ over $|B_V|$. Consider two extreme cases where we only tile the topology ($|B_F| = 1, |B_V| = B$) as in Figure 8 (left), versus only tiling the feature matrix ($|B_F| = B, |B_V| = 1$) as in Figure 8 (right), such that the working set sizes are equal. Substituting the values into Eq. 3 and finding the condition for the former being smaller than the latter,

$$\begin{aligned} B|V| + |E| + B|V||F| &> B(|V| + |E|) + |V||F|, \\ |F| &> |E|/|V|. \end{aligned} \quad (4)$$

In the above equation, $|E|/|V|$ is the average degree of the graph, one of the representative parameters of graph data. It is widely known that the average degree of real-world graphs is usually only around 10-20 [27]. Comparing this to $|F|$ being several hundreds, favoring increasing $|B_F|$ first can be a rational choice.

5 MULTI-CHIP SCALING

Figure 9 (a) illustrates the multi-chip environment. In multi-chip scaling, we assume that each chip is packaged with its own memory module such as HBM. With such an environment, the scaling challenge is that communications need to be explicit because the memories are not shared. Figure 9 (b) and (c) show the strategy for scaling. For the combination (b), we duplicate W in the memory of each chip. This is feasible since W is small. Then X is split horizontally, such that each chip can produce its own piece of the output matrix.

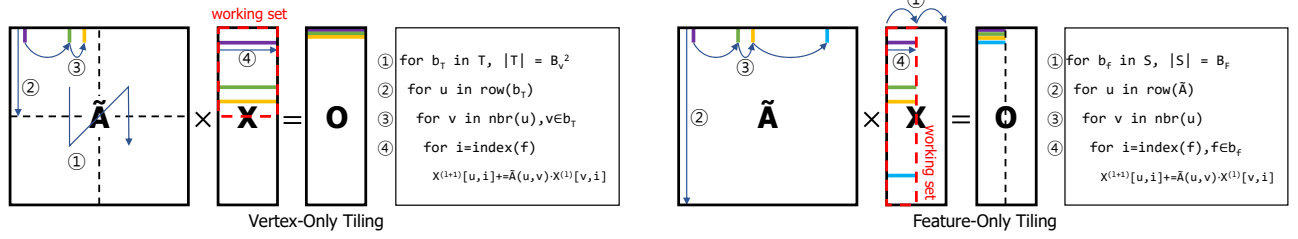


Figure 8: Two extreme cases of loop tiling for vertex-only tiling (left) and feature-only tiling (right).

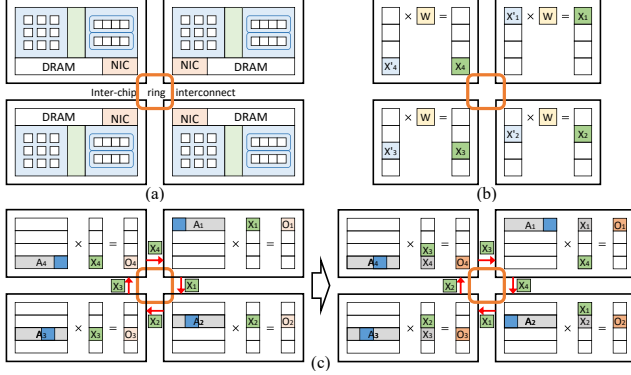


Figure 9: Multi-chip scaling strategy.

Table 1: Benchmark Dataset Information

Dataset	#Vertices	#Edges	#Features	Topology	Feature
Products (PD)	2.45 M	61.9 M	100	0.24 GB	0.91 GB
Citation (CT)	2.93 M	30.6 M	128	0.12 GB	2.79 GB
Pokec (PK)	1.63 M	30.6 M	256	0.12 GB	1.56 GB
YouTube (YT)	1.13 M	2.99 M	256	0.02 GB	1.08 GB
LiveJournal (LJ)	4.85 M	69.0 M	256	0.28 GB	4.63 GB
Orkut (OK)	3.07 M	117 M	256	0.45 GB	2.93 GB
Reddit (RD)	0.23 M	114 M	602	0.43 GB	0.52 GB

For aggregation, the topology \tilde{A} is similarly split into four pieces, and does not need to be communicated between the chips. However, X needs to be communicated because each chip only has a part of X but eventually needs the whole matrix. In our strategy as in Figure 9 (c) similar to all-gather [68], each chip starts by aggregating only with the current piece of X . At the same time, the same piece is passed to the neighboring chip in the ring. Next, the data that has been just received piece is being processed and passed to the neighbor. After $N - 1$ steps for N chips, the aggregation is complete. Note that there is no further communication after aggregation (Except for the last GCN layer), because the split output will be directly used as split input to the next layer’s combination.

6 EVALUATION

6.1 Dataset

We use seven large graph datasets from the real world as benchmarks. The details are listed in Table 1. Products (PD) is from Open

Graph Benchmark Collection [27]. It has 2.45 M vertices that represent Amazon products with 61.9 M edges which indicates products being purchased together. Each vertex has word embeddings of width 100 as features, generated from product descriptions. Citations (CT) is also from the Open Graph Benchmark Collection and represent 2.93M papers as vertices and their citations as 30.6M edges from Microsoft Academic Graph [71]. Each vertex is associated with word embeddings from their titles and abstracts. Pokec (PK), YouTube (YT), LiveJournal (LJ), Orkut (OK) and Reddit (RD) are from Stanford Large Network Dataset Collection [42]. Pokec [67] is a social network graph from Slovakia, and includes 1.63M users as vertices and 30.6M connections as edges. Youtube [77] is graph from users of a video sharing service, with 1.13M users and 2.99M connections between them. Livejournal [43] and Orkut are from online social network services with 4.85M and 3.07M vertices, respectively. Reddit [76] is a social network service, and 0.23M vertices are collected from the Reddit discussion forum. The features of the Reddit dataset consist of 302-dimensional post information, and GloVe CommonCrawl [56] based 300-dimensional word embedding vectors. For others, the node embedding vectors of width 256 have been generated from node2vec [20] and used as features.

6.2 Methodology

We evaluate the performance of SnF architecture with the configuration listed in Table 2. The accelerator runs in 1GHz frequency, where the combination engine has 32×32 systolic array and the aggregation engine has 16-way SIMD cores. Both engines use 32bit fixed point arithmetic operations.

We use HyGCN as baseline architecture, as HyGCN has an easily expandable architecture for vertex tiling and feature slicing. On the other hand, GCNAX uses static vertex tiling by pre-profiling the workload and AWB-GCN does not use caches for exploiting locality. Therefore, applying SnF which uses dynamic strategy and cache on such architectures would be infeasible.

We conduct the experiments in total of three different settings. In our default setting, a multi-engine configuration is used, which comprises eight of both engines, with an HBM2 memory subsystem. In our small scale setting, we show that SnF is also efficient on a design with small resource budget and low memory bandwidth. The setting includes one of both engines with a 4-rank DDR4 channel. Lastly, we demonstrate the extension to the multi-chip scaling method described in Section 5. We use one to 32 chips connected in a ring topology network. Following other MCM accelerators [5, 63] we use 256GB/s bandwidth ring interconnect, with 20 ns per-hop latency, where each chip is connected to its own HBM module. To

Table 2: System Configuration

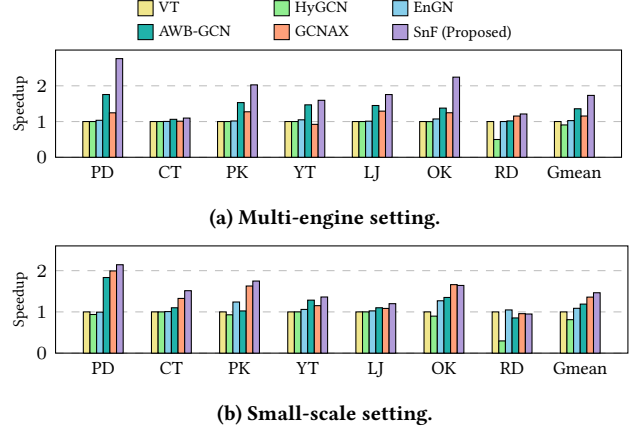
Common	Accelerator Engine	Frequency Combination Aggregation	1GHz 32×32 Syst. Array 16-Way SIMD
	Global Cache	Capacity Ways Replacement	16MB 16 LRU
Multi-engine	#Engines	Aggregation Combination	8 8
	Off-chip Memory (Shared)	Spec. Peak Bandwidth Channels Banks	HBM2 256 GB/s 8 4×4
Small scale	#Engines	Aggregation Combination	1 1
	Off-chip Memory	Spec. Peak Bandwidth Ranks Banks	DDR4-2666 21.3 GB/s 4 4×4
Multi-Chip Module	#Modules	Accelerator HBM	1-32 1-32
	Interconnect	Topology Bandwidth Latency	Ring 256 GB/s 20 ns

Table 3: Comparison of Existing GCN Accelerators

Scheme	Dataflow	Loop Tiling		Tiling Configuration	
		Topology	Feature	Method	Non-perfect Tiling
HyGCN	Row Product	✗	✗	✗	N/A
EnGN	Row Product	✗	✓	✗	N/A
AWB-GCN	Col. Product	✓	✓	✗	N/A
GCNAX	Row Product	✓	✓	Preproc.	✗
SnF (Proposed)	Row Product	✓	✓	ATM (Runtime)	✓

validate the design, we implemented the accelerator in Verilog HDL and synthesized it using Cadence Genus with 45 nm OpenPDK library, which was scaled to 32 nm. To model the on-chip memory, we used CACTI [69] to draw the power and area under 32 nm technology node. The baseline chip resembling HyGCN [75] consumed 11.40 mm², and SnF has an area of 11.55 mm². For comparison we reproduced GCNAX [46] and AWB-GCN [17], which consumed 11.23 mm² and 13.80 mm², respectively.

For performance modeling, we ported SCALE-Sim [61] to C++, and extended it to support the SnF’s aggregation unit. The cycles were matched to that of the RTL model. For modeling the DRAM subsystem, we used DRAMsim3 [49]. We faithfully reproduced the previous work from Table 3. HyGCN [75] is the baseline accelerator with hybrid engines, and EnGN [50] proposes an RER dataflow with DAVC that captures high-degree vertices. AWB-GCN [17] is based on column product which utilizes same set of PEs for both aggregation and combination with separate task distributors. Lastly, GCNAX [46] perform a static analysis to find the optimal loop tiling under the assumption of perfect tiling. For comparison, we also added a ‘VT’ version of the accelerator, to which we normalized all values.

**Figure 10: Performance of SnF in (a) multi-engine setting and (b) small-scale setting.**

6.3 Multi-Engine Accelerator Results

In this subsection, we analyze the multi-engine performance to show the proposed SnF outperforms the existing accelerators. We placed eight engines into the accelerator, with HBM2 memory providing 256 GB/s peak bandwidth. The results are shown in Figure 10a. We set ‘VT’ as a baseline which only performs vertex tiling. ‘SnF’ is the proposed accelerator with the feature slicing on top of vertex tiling with automatic tile morphing. Among the multiple engines, we split the graph workload such that the number of edges per engine is equal. For all implementations except SnF which is dynamic, we examined all possible partitioning combinations off-line (i.e., optimal) and chose the best one.

Comparing SnF with VT gives an insight into how much benefit can be drawn from choosing the right loop tiling scheme for GCN inference. The performance improvement of SnF over VT is 73.1%, obtained by reducing the significant amount overhead of VT’s repetitive feature access cost and dynamically finding the right configuration. The largest speedup is on PD with 2.76×, coming from the fact that the optimal setting of VT was at a large $B_V = 64$. This large B_V makes a huge repetition overhead to the output feature accesses. Feature slicing can efficiently split these repetition counts, contributing to the superior speedup.

The proposed technique outperforms loop tiling strategies from the existing prior designs in all datasets. HyGCN adopts no tiling, and shows a poor cache efficiency. EnGN is based on vertex tiling, and uses DAVC to capture features from high-degree vertices. However, we have found that the DAVC has a marginal effect on the speedup. One reason is that there are too many high-degree vertices in the large-scale real-world graph datasets for DAVC to capture. Moreover, when their reuse distances are short enough, they are often already well-captured by the default LRU replacement policy. AWB-GCN is unique among the designs under test in that they utilize column product based execution with an aggressive load balancing. It requires a non-negligibly large output buffer to function without a separate consideration for spilling, given that there are a few million vertices in the graph. Even though AWB-GCN splits the matrix, it adds the repetition counts on the feature accesses,

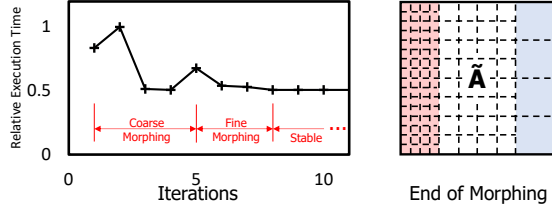


Figure 11: Example automatic tile morphing over iterations.

which becomes a reason to underperform SnF by 35.7%. GCNAX provides an analytic model for finding the optimal partitioning scheme, and it provides 15.4% speedup over VT. However, they only consider perfect tiling in their model, missing an important opportunity for performance enhancements. Moreover, because they unrealistically assume uniformly distributed sparse graphs, their model is often distant from the real measurements and this becomes another source of 68.2% performance loss compared to SnF.

Figure 11 shows how automatic tile morphing performs over the repetitions in PK dataset. The first four iterations are coarse morphing. It gradually checks multiple B_V values and settles at $B_V = 8$. The overhead from these non-optimal executions is amortized over multiple iterations. In the fine morphing, it ends up further splitting the first column which has the lowest hit rate, and merging the last two columns which have the highest hit rate in our experiments, automatic tile morphing was able to obtain over 95% the performance that could be obtained by the optimal analysis, which is an unavailable information at runtime.

6.4 Small-Scale Accelerator Results

In this subsection, we analyze the single-engine accelerator performance to show that feature slicing and automatic tile morphing are also effective for systems under tight resource budget such as mobile and embedded systems. Figure 10b shows the small scale performance of the GCN execution.

As in multi-engine settings, SnF outperforms all prior designs. One interesting aspect is that among the prior designs GCNAX performs better than AWB-GCN in the small scale setting. In this setting, the available memory bandwidth is quite small, and it becomes crucial to utilize the cache efficiently. Because AWB-GCN does not have particular caching mechanism, the benefit of better utilizing the cache becomes more important than load balancing. SnF still finds better settings on all datasets except for OK and RD, with 10.8% improvement over GCNAX and 46.4% over VT.

Reddit shows a unique trend for performance speedup because it has the largest number of edges per vertex (dense topology) among the datasets while having fewer vertices. The dense topology of RD works well with VT, as illustrated in Figure 10, in which VT shows superior speedup over HyGCN. Also, fewer vertices require a smaller feature matrix than other datasets, which diminishes the output write overhead of VT. GCNAX uses perfect tiling, so it constructs a too large B_V tiling strategy, which makes lower speedup over VT. For SnF, the dynamic tiling found by the automatic tile morphing is almost equal to that of the static solution found by GCNAX. Because automatic tile morphing takes some iterations

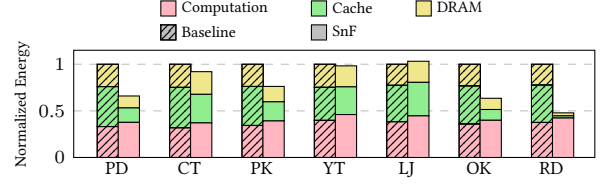


Figure 12: Normalized energy consumption breakdown of baseline (shaded) and SnF (solid).

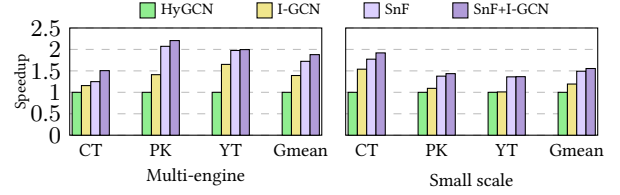


Figure 13: Performance of I-GCN reordering.

to settle around the best solution, a slight speedup degradation of 0.82% over GCNAX occurs for SnF as depicted in Figure 10b. OK is also as dense as Reddit, but it has many vertices. This environment is not friendly for VT. So, both GCNAX and SnF outperform VT, unlike the Reddit case. SnF has a minor speedup degradation of 1.8% over GCNAX, similar to Reddit.

6.5 Energy Consumption

Figure 12 shows the normalized energy consumption of the aggregation phase with the breakdown, under the single chip, multi-engine setting. We set the baseline as the architecture with no partitioning, whose energy consumption is depicted with shaded bars. The energy consumption of the SnF is represented by the solid bars. As indicated in the figure, SnF consumes slightly more energy on computation, but much more energy is saved from the memory and the cache. These both show the efficient usage of cache in SnF due to the increased cache hit rate, because less data is read from the DRAM, and less data is written to the cache. An exception is LJ, where the benefit from cache and DRAM is slightly less than the increased energy in computation. We can save 53% energy on RD because it has an extremely dense topology structure that accompanies a smaller topology access ratio over feature accesses. Therefore, since SnF can significantly reduce feature accesses, the energy consumption is greatly reduced.

6.6 Effect of Reordering

Another promising scheme for enhancing cache efficiency for GCNs is graph reordering as adopted in Rubik [11] and I-GCN [18]. SnF is able to take further benefit from those reordering schemes, due to two reasons. First, when a graph is reordered, it forms small, dense clusters. In consequence, the access pattern becomes similar to that of a smaller working set. This would change the optimal number of vertex tiles, but SnF is able to adapt to it thanks to automatic tile morphing. Second, reordering helps improve the locality of the accesses. Because SnF is a technique that exploits the locality of accesses using caches, reordering often strengthens SnF.

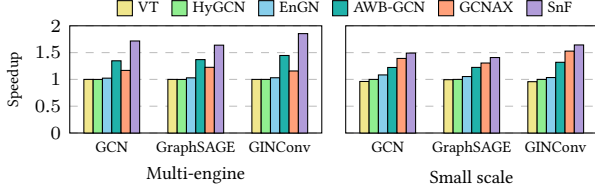


Figure 14: Performance of variant GNN application.

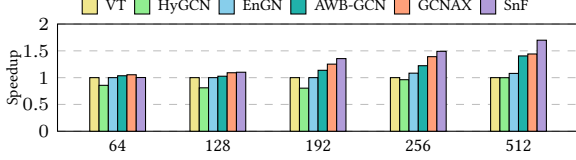


Figure 15: Performance of the SnF for various feature widths.

Figure 13 plots the performance benefit of SnF implemented with reordering of I-GCN [18] on three datasets. As depicted in the graphs, combining reordering and SnF consistently add extra speedup over using each scheme on its own. On multi-engine setting, combination of the reordering and SnF adds 87.9% improvement on top of I-GCN in geometric mean, and 4.22% over original SnF in geometric mean. On the small scale setting, the improvement is 55.4% over I-GCN and 9.04% over original SnF.

6.7 Performance on GCN Variants

Although SnF focuses on acceleration of GCNs, there are many variants of GCNs [23, 74] and SnF can be used to execute them. We implement two popular GCN variants, GraphSAGE [23] and GINConv [74], which pose slight modification to the aggregation phase. Figure 14 plots the performance of GCNs. Each result shows almost identical trend, because they share the same aggregation-combination structure. On GraphSAGE, SnF gets 63.9% speedup over VT in multi-engine setting and 40.7% in small scale setting. On the other hand, on GINConv, SnF gets 85.4% in multi-engine and 64.3% in small scale setting. Because GraphSAGE applies sampling that minimize the number of edge access which reduces the chance for feature reuse, its performance gain are slightly lower than in GCN. On the other hand, GINConv uses smaller set of edge weights (that is part of \tilde{A}), and thus speedup from reading the features become more prominent, leading to a higher speedup than GCN.

6.8 Sensitivity to Feature Width

In this subsection, we provide sensitivity analyses of the SnF. One insight from Eq. 4 is that speedup of feature slicing depends on B_F . Figure 15 presents performance sensitivity to the feature widths in geometric mean. As indicated in the figure, the effectiveness of SnF is reduced with the layers of small feature widths which often appear in the later layers of GCNs. However, the impact of such layers would be marginal due to short execution times. Furthermore, the configuration found by SnF can be reused in the succeeding layers. With the trend of wider feature width and deeper layers, the benefit of ATM is likely to strengthen over time.

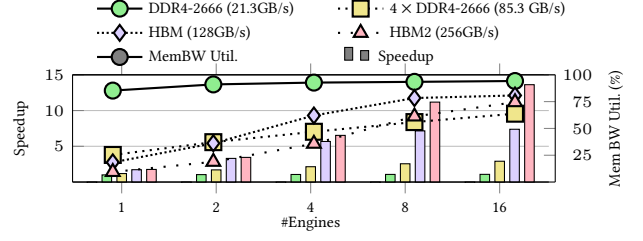


Figure 16: Sensitivity of SnF to the various memory systems and the number of engines.

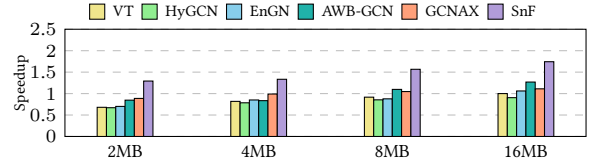


Figure 17: Performance (geomean) of the SnF for various cache sizes.

6.9 Sensitivity to System

Figure 16 shows how SnF performs with various number of engines and various memory systems, normalized at the performance of a small scale SnF with a DDR4-2666 channel. With one DDR4-2666 channel peaked at 21.3GB/s, increasing the number of engines gives diminishing returns, as the execution becomes memory bound. However, with memory subsystems with higher bandwidth, it requires more engines to fill the bandwidth. For example, an HBM2 system that provides 256GB/s can gain from more processing engines, and exhibit almost linear speedup until eight engines. Afterwards it reaches the saturation point. Based on the study, we set the number of engines in the default setting to be eight.

6.10 Sensitivity to Cache Size

Analyzing the cache size sensitivity is essential because SnF takes advantage of efficient cache locality. Figure 17 shows the performance of SnF for various cache sizes. SnF generally outperforms other architectures. SnF is especially advantageous in a small cache setting, so it works well with a smaller cache size to reduce silicon area. In a small cache setting, the miss ratio of feature access, which SnF targets to minimize, increases, so SnF provides more speedup over other accelerators. For example, in the 2MB setting, SnF shows 96.7% improvement over VT, while the improvement of the 16MB setting is 73.1% which is still a significant speedup.

6.11 Sensitivity to Cache Configuration

Figure 18 shows the sensitivity to various cache configurations, including replacement policies, number of ways, and block size. For replacement, we have tested random and RRIP [84]. Random replacement resulted in an surprisingly worse speedup, due to its inability to capture the locality. RRIP was able to gain a marginal amount of speedup, but it was not enough to justify the additional cost for storing more states. While number of ways did not provide

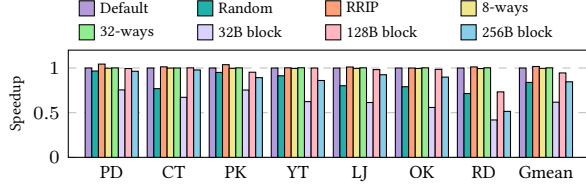


Figure 18: Sensitivity to various cache configurations.

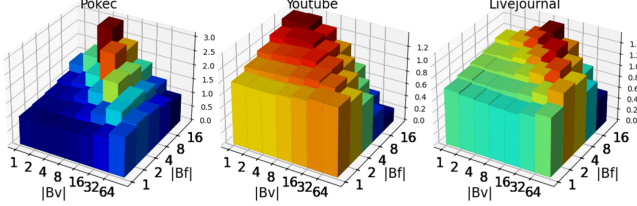


Figure 19: Sensitivity on B_F and B_V .

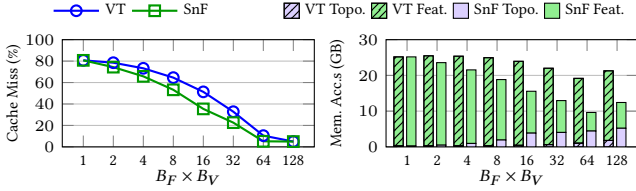


Figure 20: Miss rate (left) and memory access (right) according to $B_F \times B_V$.

much changes, block sizes altered much performance. When decreased, it becomes lower than the size of the DRAM burst, wasting a lot of the bandwidth. When increased, the size exceeded the trivial spatial locality of the feature slicing, and the speedup degraded.

6.12 Sensitivity on B_F and B_V

Figure 19 shows the sensitivity of SnF with respect to B_F and B_V on three selected datasets. The results exemplify the difficulty of tuning the number of vertex tiles B_V . The optimal configuration is usually found on $B_F=16$ (the maximum), which supports our strategy to use feature slicing and then to adaptively find optimal B_V . B_V , on the other side, is harder to tune since it depends too much on the individual graph topology. Larger graphs favor larger B_V because larger graphs would be harder to fit into caches.

Figure 20 (left) shows the cache miss rate, with respect to $B_F \times B_V$ observed for PK dataset. The miss rate decreases as $B_F \times B_V$ becomes larger as the working set size decreases. The miss rate drops for VT only and SnF are mostly similar, showing that our assumption for the cost model generally holds in that the miss rate is roughly a function of the working set size.

Figure 20 (right) shows the memory access count breakdown that explains how the miss rates and repetition counts are translated into performance. The green bars represent the feature accesses, and the purple bars represent the topology data accesses. In vertex tiling, the repetition count being added to the output feature accesses offsets the gain from the miss rate drop and results in a diminishing return. However, with SnF, the miss rate drop is almost directly

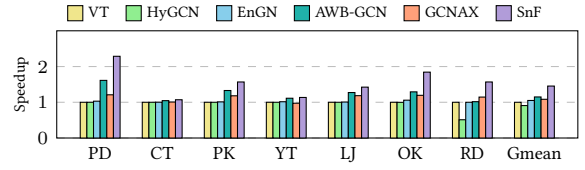


Figure 21: Performance of the multi-chip accelerator.

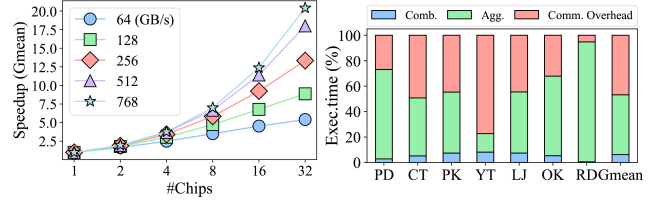


Figure 22: Multi-chip scaling results (left) and execution time breakdown (right).

translated into memory access reduction as the repetition is added to smaller topology data.

6.13 Multi-Chip Module Scaling Results

Figure 21 shows the multi-chip-module (MCM) accelerator performance where 16 chips in total form a module. Following other MCM accelerators [5, 63] we use 256 GB/s bandwidth ring interconnect, with 20 ns per-hop latency. Even though all accelerators use the same strategy explained in Section 5, SnF achieves superior speedup over all others. Further scaling results are provided in Figure 22. On the left, it plots the scalability according to the interconnect bandwidth. Using interconnect with high bandwidth, it scales to some degree, but its speedup is limited for low-bandwidth interconnects. On the right, the figure shows the breakdown of combination, aggregation and the communication overhead not hidden by the overlap.

The data with a large average degree such as PD, OK and RD scale well, because the communication time depends on the features per vertex and the computation time generally is proportional to the number of edges. On the other hand, low-degree graph such as YT shows poor scalability due to the low average degree and thus high communication overhead.

6.14 Experiments on Small-Scale Datasets

In addition to the datasets we evaluated, there exist some small-scale datasets often evaluated in some prior art [17, 46, 75]: Cora, Citeseer [62], Pubmed [22], and Nell [9]. To make a fair comparison, we also report performance on those datasets in Figure 23. We used 512 KB cache sizes for all architectures following [46]. The performance improvement of SnF over the baseline is 106%, which is much larger than the results SnF gets from large datasets, as depicted in Figure 23a. The results align with the observations from previous work [17, 46]. However, we do not use these small-scale datasets for our main evaluation because these datasets often contain only a few thousands of vertices and thus consume tiny cycles to compute GCN compared to larger ones, as illustrated in Figure 23b.

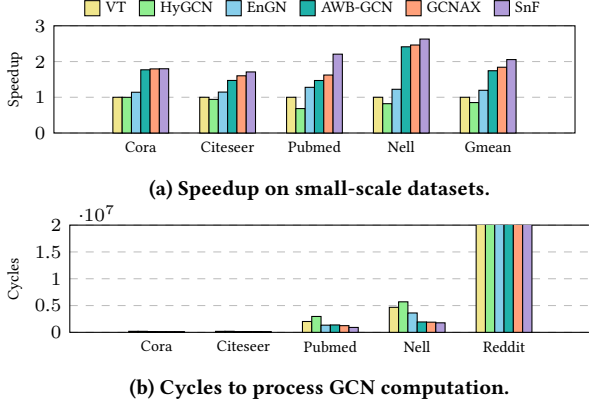


Figure 23: Results on small-scale datasets.

7 RELATED WORK

7.1 Accelerators for GCN and Graph Processing

There are many existing architectural approaches that aim to accelerate GCNs. HyGCN [75] proposed the hybrid computation architecture using the characteristic difference in the aggregation and the combination phase in GCNs. GNNA [8] used a tiled architecture to accelerate GCN. EnGN [50] adopted a tiled topology data and gathered information about highly visited vertices to allocate some portion of cache for them to enhance cache efficiency. Moreover, GCNAX [46] uses a perfect tiling strategy by doing off-line analysis, which finds the best dataflow and tiling configuration. However, their perfect tiling over-estimates a required buffer size, leading to suboptimal performance. In contrast, this paper focuses on cache efficiency and claims that feature slicing often provides a better efficiency than prior solutions. AWB-GCN [17] used column-based execution and gave insight into distributing workload. Recent work also supports variants of GCNs that integrate the edge information or self-attention into GCNs. SnF shows a similar speedup for such GCN variants because feature slicing and dynamic analysis technology can be easily applied without much challenge.

Not only GCNs, but classic graph processing has been an important application for decades, and there were various works which propose dedicated accelerators. They utilized ASICs [21, 53, 80], FPGAs [7, 13, 40], or both [10] to implement these accelerators. Focusing on their memory-intensive nature, there were accelerators that utilize 3D-stacked memories [55] as a processing-in-memory accelerator [1, 82, 90], or modify flash storage to be friendly for graph processing.

Unfortunately, the computational pattern of such classic graph processing is distinct from that of the GCNs, because the features associated with each vertex is often shallow, with one or two elements per vertex. Because GCNs exhibit hybrid computational pattern and the feature vector associated with each vertex is relatively long, GCN accelerators require different design from that of the graph processing accelerators.

7.2 Memory Aware Accelerators for DNNs

DNN acceleration often accompanies memory-bound operations, so many works optimize memory bandwidth for successful speedup [31,

59, 65]. Some works precisely select the dataflow [12, 15, 34] or block data [78] to improve data reuse. On-chip memory management is also crucial for optimization. Many works try to efficiently deal with on-chip memory by scheduling, allocation, or sharing [33, 47, 73]. DNNs often include of multiple layers, which can be utilized to optimize memory usage [4, 30, 36, 51]. This characteristic can be adopted not only for inference [4, 30] and training [51] but also for batch normalization [36].

These methods apply to the regular access pattern of conventional DNNs, which is not directly applicable to GCNs. Therefore, GCN accelerator designs are different from conventional DNN accelerator designs because they target the irregular accesses.

7.3 Sparse DNN Accelerators

Some DNN accelerators attempt to utilize sparsity in DNNs. Computation pruning [28, 52, 64] was a popular target because it can easily apply to existing hardware designs. Sparse operation support [72, 88] or algebraic sparsity exploration [29] were also studied. There are also zero-value aware designs, such as removing zero-value weights [3, 14, 24, 83, 87] or considering zero-value activations [19, 32, 35, 54]. Some designs target SpMV [6, 60] and SpMM [25, 58, 85], which can be used to exploit sparsity in DNNs. In addition, some works [37, 57, 66, 79] co-designed software and hardware for tensor compression. However, the sparsity targeted from these work is often far below that of the GCNs, because the sparsity of graph topology is near 100%, which is difficult for pruned DNNs or zero-valued activations to reach. Therefore, despite the much work on sparse DNN accelerations, there exists a need for dedicated GCN accelerators.

8 CONCLUSION

We have proposed slice-and-forge, an accelerator design oriented at efficiently utilizing the caches for GCN accelerators. With feature slicing, slice-and-forge greatly improves the effectiveness of the limited on-chip cache compared to previous work. Taking advantage of the fact that feature slicing yields multiple exact same computational patterns, we further propose automatic tile morphing that dynamically configures the tiling for better cache efficiency. Experimental results show that slice-and-forge achieves superior performance over the existing designs, and provides relaxation for the need for off-line analysis.

ACKNOWLEDGMENTS

This work was partly supported by the National Research Foundation of Korea (NRF) grants (2022R1C1C1011307, 2022R1C1C1008131) and Institute of Information & communications Technology Planning & Evaluation (IITP) grants (2021-0-00853, 2020-0-01361) funded by the Korea government (MSIT). The EDA tool was supported by the IC Design Education Center (IDEC), Korea. Mingi Yoo, Jaeyong Song, Hyeyoon Lee, Jounghoo Lee, and Youngsok Kim are with the Department of Computer Science at Yonsei University and have been partly supported by the BK21 FOUR (Fostering Outstanding Universities for Research) funded by the Ministry of Education (MOE, Korea) and National Research Foundation of Korea (NRF).

REFERENCES

- [1] Junwhan Ahn, Sungpack Hong, Sungjoo Yoo, Onur Mutlu, and Kiyoungh Choi. 2015. A scalable processing-in-memory accelerator for parallel graph processing. In *ISCA*.
- [2] Hasan Metin Aktulga, Aydin Buluç, Samuel Williams, and Chao Yang. 2014. Optimizing sparse matrix-multiple vectors multiplication for nuclear configuration interaction calculations. In *IPDPS*.
- [3] Jorge Albericio, Patrick Judd, Tayler Hetherington, Tor Aamodt, Natalie Enright Jerger, and Andreas Moshovos. 2016. Cnvlutin: Ineffectual-Neuron-Free Deep Neural Network Computing. In *ISCA*.
- [4] Manoj Alwani, Han Chen, Michael Ferdman, and Peter Milder. 2016. Fused-layer CNN accelerators. In *MICRO*.
- [5] Akhil Arunkumar, Evgeny Bolotin, Benjamin Cho, Ugljesa Milic, Eiman Ebrahimi, Oreste Villa, Aamer Jaleel, Carole-Jean Wu, and David Nellans. 2017. MCM-GPU: Multi-chip-module GPUs for continued performance scalability. *MICRO* 45, 2 (2017), 320–332.
- [6] Bahar Asgari, Ramyad Hadidi, Tushar Krishna, Hyesoon Kim, and Sudhakar Yalamanchili. 2020. ALRESCHA: A Lightweight Reconfigurable Sparse-Computation Accelerator. In *HPCA*.
- [7] Mikhail Asiaty and Paolo Ienne. 2021. Large-Scale Graph Processing on FPGAs with Caches for Thousands of Simultaneous Misses. In *ISCA*.
- [8] Adam Auten, Matthew Tomei, and Rakesh Kumar. 2020. Hardware acceleration of graph neural networks. In *DAC*.
- [9] Andrew Carlson, Justin Betteridge, Bryan Kisiel, Burr Settles, Estevam R. Hruschka, and Tom M. Mitchell. 2010. Toward an Architecture for Never-Ending Language Learning. In *Proceedings of the Twenty-Fourth AAAI Conference on Artificial Intelligence* (Atlanta, Georgia) (AAAI’10). AAAI Press, 1306–1313.
- [10] Xuhao Chen, Tianhao Huang, Shuotao Xu, Thomas Bourgeat, Chanwoo Chung, and Arvind. 2021. FlexMiner: A Pattern-Aware Accelerator for Graph Pattern Mining. In *ISCA*.
- [11] Xiaobing Chen, Yuke Wang, Xinfeng Xie, Xing Hu, Abanti Basak, Ling Liang, Mingyu Yan, Lei Deng, Yufei Ding, Zidong Du, Yunji Chen, and Yuan Xie. 2020. Rubik: A Hierarchical Architecture for Efficient Graph Learning. *CoRR* abs/2009.12495 (2020). [arXiv:2009.12495](https://arxiv.org/abs/2009.12495) <https://arxiv.org/abs/2009.12495>
- [12] Yu-Hsin Chen, Tushar Krishna, Joel S Emer, and Vivienne Sze. 2016. Eyeriss: An energy-efficient reconfigurable accelerator for deep convolutional neural networks. *JSSC* (2016).
- [13] Vidushi Dadu, Sihao Liu, and Tony Nowatzki. 2021. PolyGraph: Exposing the Value of Flexibility for Graph Processing Accelerators. In *ISCA*.
- [14] Caiwen Ding, Siyu Liao, Yanzhi Wang, Zhe Li, Ning Liu, Youwei Zhuo, Chao Wang, Xuehai Qian, Yu Bai, Geng Yuan, Xiaolong Ma, Yipeng Zhang, Jian Tang, Qinru Qiu, Xue Lin, and Bo Yuan. 2017. CirCNN: Accelerating and Compressing Deep Neural Networks Using Block-Circulant Weight Matrices. In *MICRO*.
- [15] Zidong Du, Robert Fasthuber, Tianshi Chen, Paolo Ienne, Ling Li, Tao Luo, Xiaobing Feng, Yunji Chen, and Olivier Temam. 2015. ShiDianNao: Shifting vision processing closer to the sensor. In *ISCA*.
- [16] Alex Fout, Jonathon Byrd, Basir Shariat, and Asa Ben-Hur. 2017. Protein interface prediction using graph convolutional networks. In *NeurIPS*.
- [17] Tong Geng, Ang Li, Runbin Shi, Chunshu Wu, Tianqi Wang, Yanfei Li, Pouya Haghi, Antonino Tumeo, Shuai Che, Steve Reinhardt, and Martin C. Herbordt. 2020. AWB-GCN: A graph convolutional network accelerator with runtime workload rebalancing. In *MICRO*.
- [18] Tong Geng, Chunshu Wu, Yongan Zhang, Cheng Tan, Chenhao Xie, Haoran You, Martin Herbordt, Yingyan Lin, and Ang Li. 2021. I-GCN: A Graph Convolutional Network Accelerator with Runtime Locality Enhancement through Islandization. In *MICRO*. Association for Computing Machinery, New York, NY, USA, 1051–1063. <https://doi.org/10.1145/3466752.3480113>
- [19] Ashish Gondimalla, Noah Chesnut, Mithuna Thottethodi, and T. N. Vijaykumar. 2019. SparTen: A Sparse Tensor Accelerator for Convolutional Neural Networks. In *MICRO*.
- [20] Aditya Grover and Jure Leskovec. 2016. node2vec: Scalable feature learning for networks. In *KDD*.
- [21] Tae Jun Ham, Lisa Wu, Narayanan Sundaram, Nadathur Satish, and Margaret Martonosi. 2016. Graphiconado: A high-performance and energy-efficient accelerator for graph analytics. In *MICRO*.
- [22] Will Hamilton, Zhitao Ying, and Jure Leskovec. 2017. Inductive Representation Learning on Large Graphs. In *Advances in Neural Information Processing Systems*, I. Guyon, U. Von Luxburg, S. Bengio, H. Wallach, R. Fergus, S. Vishwanathan, and R. Garnett (Eds.), Vol. 30. Curran Associates, Inc. <https://proceedings.neurips.cc/paper/2017/file/5dd9db5e033da9c6fb5ba83c7a7e9ea9-Paper.pdf>
- [23] William L Hamilton, Rex Ying, and Jure Leskovec. 2017. Inductive representation learning on large graphs. In *NeurIPS*.
- [24] Song Han, Xingyu Liu, Huizi Mao, Jing Pu, Ardavan Pedram, Mark A Horowitz, and William J Dally. 2016. EIE: Efficient Inference Engine on Compressed Deep Neural Network. In *ISCA*.
- [25] Kartik Hegde, Hadi Asghari-Moghaddam, Michael Pellauer, Neal Crago, Aamer Jaleel, Edgar Solomonik, Joel Emer, and Christopher W Fletcher. 2019. ExTensor: An accelerator for sparse tensor algebra. In *MICRO*.
- [26] Changwan Hong, Aravind Sukumaran-Rajam, Israt Nisa, Kunal Singh, and P Sadayappan. 2019. Adaptive sparse tiling for sparse matrix multiplication. In *PPoPP*.
- [27] Weihua Hu, Matthias Fey, Marinka Zitnik, Yuxiao Dong, Hongyu Ren, Bowen Liu, Michele Catasta, and Jure Leskovec. 2020. Open graph benchmark: Datasets for machine learning on graphs. *arXiv preprint* (2020).
- [28] Weizhe Hua, Yuan Zhou, Christopher De Sa, Zhiru Zhang, and G. Edward Suh. 2019. Boosting the Performance of CNN Accelerators with Dynamic Fine-Grained Channel Gating. In *MICRO*.
- [29] Chao-Tsung Huang. 2021. RingCNN: Exploiting Algebraically-Sparse Ring Tensors for Energy-Efficient CNN-Based Computational Imaging. In *ISCA*.
- [30] Chao-Tsung Huang, Yu-Chun Ding, Huan-Ching Wang, Chi-Wen Weng, Kai-Ping Lin, Li-Wei Wang, and Li-De Chen. 2019. eCNN: A block-based and highly-parallel CNN accelerator for edge inference. In *MICRO*.
- [31] Bongjoon Hyun, Youngeun Kwon, Yujeong Choi, John Kim, and Minsoo Rhu. 2020. NeuMMU: Architectural Support for Efficient Address Translations in NPU. In *ASPLOS*.
- [32] Jun-Woo Jang, Sehwan Lee, Dongyoung Kim, Hyunsun Park, Ali Shafiee Ardestani, Yeongjae Choi, Channoh Kim, Yoojin Kim, Hyeonseok Yu, Hamzah Abdel-Aziz, Jun-Seok Park, Heonsoo Lee, Dongwoo Lee, Myeong Woo Kim, Hanwoong Jung, Heewoo Nam, Dongguen Lim, Seungwon Lee, Joon-Ho Song, Suknam Kwon, Joseph Hassoun, SukHwan Lim, and Changkyu Choi. 2021. Sparsity-Aware and Re-configurable NPU Architecture for Samsung Flagship Mobile SoC. In *ISCA*.
- [33] Tian Jin and Seokin Hong. 2019. Split-CNN: Splitting window-based operations in convolutional neural networks for memory system optimization. In *ASPLOS*.
- [34] Norman P. Jouppi, Cliff Young, Nishant Patil, David Patterson, Gaurav Agrawal, Raminder Bajwa, Sarah Bates, Suresh Bhatia, Nan Boden, Al Borchers, Rick Boyle, Pierre-luc Cantin, Clifford Chao, Chris Clark, Jeremy Coriell, Mike Daley, Matt Dau, Jeffrey Dean, Ben Gelb, Tara Vazir Ghaemmaghami, Rajendra Gottipati, William Gulland, Robert Hagmann, C. Richard Ho, Doug Hogberg, John Hu, Robert Hundt, Dan Hurt, Julian Ibarz, Aaron Jaffey, Alek Jaworski, Alexander Kaplan, Harshit Khaitan, Daniel Killebrew, Andy Koch, Naveen Kumar, Steve Lacy, James Laudon, James Law, Diemthu Le, Chris Leary, Zhuyuan Liu, Kyle Lucke, Alan Lundin, Gordon MacKean, Adriana Maggiore, Maire Mahony, Kieran Miller, Rahul Nagarajan, Ravi Narayanaswami, Ray Ni, Kathy Nix, Thomas Norrie, Mark Omernick, Narayana Penukonda, Andy Phelps, Jonathan Ross, Matt Ross, Amir Salek, Emad Samadiani, Chris Severn, Gregory Sizikov, Matthew Snellman, Jed Souter, Dan Steinberg, Andy Swing, Mercedes Tan, Gregory Thorson, Bo Tian, Horia Toma, Erick Tuttle, Vijay Vasudevan, Richard Walter, Walter Wang, Eric Wilcox, and Doe Hyun Yoon. 2017. In-datacenter performance analysis of a tensor processing unit. In *ISCA*.
- [35] Patric Judd, Alberto Delmas, Sayeh Sharify, and Andreas Moshovos. 2017. Cnvlutin²: Ineffectual-Activation-and-Weight-Free Deep Neural Network Computing. *arXiv preprint* (2017).
- [36] Daejin Jung, Wonkyung Jung, Byeongho Kim, Sunjung Lee, Wonjong Rhee, and Jung Ho Ahn. 2019. Restructuring batch normalization to accelerate CNN training. In *SysML*.
- [37] Konstantinos Kanellopoulos, Nandita Vijaykumar, Christina Giannoula, Roknodin Azizi, Skanda Koppula, Nika Mansouri Ghiasi, Taha Shahroodi, Juan Gomez Luna, and Onur Mutlu. 2019. Smash: Co-designing software compression and hardware-accelerated indexing for efficient sparse matrix operations. In *MICRO*.
- [38] Kevin Kinningham, Christopher Re, and Philip Levis. 2020. GRIP: A graph neural network accelerator architecture. *arXiv preprint* (2020).
- [39] Thomas N Kipf and Max Welling. 2016. Semi-supervised classification with graph convolutional networks. *arXiv preprint* (2016).
- [40] Jinho Lee, Heesu Kim, Sungjoo Yoo, Kiyoungh Choi, H Peter Hofstee, Gi-Joon Nam, Mark R Nutter, and Damir Jamsek. 2017. ExtraV: Boosting graph processing near storage with a coherent accelerator. *pVLDB* (2017).
- [41] Jure Leskovec, Jon Kleinberg, and Christos Faloutsos. 2005. Graphs over time: Densityification laws, shrinking diameters and possible explanations. In *KDD*.
- [42] Jure Leskovec and Andrej Krevl. 2014. SNAP Datasets: Stanford Large Network Dataset Collection. <http://snap.stanford.edu/data>.
- [43] Jure Leskovec, Kevin J Lang, Anirban Dasgupta, and Michael W Mahoney. 2009. Community structure in large networks: Natural cluster sizes and the absence of large well-defined clusters. *Internet Mathematics* 6, 1 (2009), 29–123.
- [44] Guohao Li, Matthias Muller, Ali Thabet, and Bernard Ghanem. 2019. DeepGCNs: Can GCNs go as deep as CNNs?. In *ICCV*.
- [45] Han Li, Mingyu Yan, Xiaocheng Yang, Lei Deng, Wenming Li, Xiaochun Ye, Dongrui Fan, and Yuan Xie. 2021. Hardware Acceleration for GCNs via Bidirectional Fusion. *IEEE Computer Architecture Letters* (2021).
- [46] Jiajun Li, Ahmed Louri, Avinash Karanth, and Razvan Bunescu. 2021. GCNAX: A flexible and energy-efficient accelerator for graph convolutional neural networks. In *HPCA*.
- [47] Jiajun Li, Guihai Yan, Wenyan Lu, Shuhao Jiang, Shijun Gong, Jingya Wu, and Xiaowei Li. 2018. SmartShuttle: Optimizing off-chip memory accesses for deep

- learning accelerators. In *DATE*.
- [48] Qimai Li, Zhichao Han, and Xiao-Ming Wu. 2018. Deeper insights into graph convolutional networks for semi-supervised learning. In *AAAI*.
 - [49] Shang Li, Zhiyuan Yang, Dhiraaj Reddy, Ankur Srivastava, and Bruce Jacob. 2020. DRAMsim3: A cycle-accurate, thermal-capable DRAM simulator. *CAL* (2020).
 - [50] Shengwen Liang, Ying Wang, Cheng Liu, Lei He, Li Huawei, Dawen Xu, and Xiaowei Li. 2020. EnGN: A high-throughput and energy-efficient accelerator for large graph neural networks. *TC* (2020).
 - [51] Sangkug Lym, Armand Behroozi, Wei Wen, Ge Li, Yongkee Kwon, and Mattan Erez. 2019. Mini-batch serialization: CNN training with inter-layer data reuse. In *SysML*.
 - [52] Wei Niu, Xiaolong Ma, Sheng Lin, Shihao Wang, Xuehai Qian, Xue Lin, Yanzhi Wang, and Bin Ren. 2020. PatDNN: Achieving Real-Time DNN Execution on Mobile Devices with Pattern-based Weight Pruning. In *ASPLOS*.
 - [53] Muhammet Mustafa Ozdal, Serif Yesil, Taemin Kim, Andrey Ayupov, John Greth, Steven Burns, and Ozcan Ozturk. 2016. Energy efficient architecture for graph analytics accelerators. In *ISCA*.
 - [54] Angshuman Parashar, Minsoo Rhu, Anurag Mukkara, Antonio Puglielli, Rangharajan Venkatesan, Bruce Khailany, Joel Emer, Stephen W. Keckler, and William J. Dally. 2017. SCNN: An Accelerator for Compressed-sparse Convolutional Neural Networks. In *ISCA*.
 - [55] J Thomas Pawlowski. 2011. Hybrid memory cube (HMC). In *Hot Chips*.
 - [56] Jeffrey Pennington, Richard Socher, and Christopher D. Manning. 2014. GloVe: Global Vectors for Word Representation. In *Empirical Methods in Natural Language Processing (EMNLP)*. 1532–1543. <http://www.aclweb.org/anthology/D14-1162>
 - [57] Lillian Pentecost, Marco Donato, Brandon Reagen, Udit Gupta, Siming Ma, Gu-Yeon Wei, and David Brooks. 2019. MaxNVM: Maximizing DNN Storage Density and Inference Efficiency with Sparse Encoding and Error Mitigation. In *MICRO*.
 - [58] Eric Qin, Ananda Samajdar, Hyoukjun Kwon, Vineet Nadella, Sudarshan Srinivasan, Dipankar Das, Bharat Kaul, and Tushar Krishna. 2020. SIGMA: A Sparse and Irregular GEMM Accelerator with Flexible Interconnects for DNN Training. In *HPCA*.
 - [59] Minsoo Rhu, Natalia Gimelshein, Jason Clemons, Arslan Zulfiqar, and Stephen W. Keckler. 2016. vDNN: Virtualized Deep Neural Networks for Scalable, Memory-Efficient Neural Network Design. In *MICRO*.
 - [60] Fazle Sadi, Joe Sweeney, Tze Meng Low, James C. Hoe, Larry Pileggi, and Franz Franchetti. 2019. Efficient SpMV Operation for Large and Highly Sparse Matrices using Scalable Multi-way Merge Parallelization. In *MICRO*.
 - [61] Ananda Samajdar, Yuhao Zhu, Paul Whatmough, Matthew Mattina, and Tushar Krishna. 2018. SCALE-Sim: Systolic CNN accelerator simulator. *arXiv preprint* (2018).
 - [62] Prithviraj Sen, Galileo Namata, Mustafa Bilgic, Lise Getoor, Brian Galligher, and Tina Eliassi-Rad. 2008. Collective Classification in Network Data. *AI Magazine* 29, 3 (Sep. 2008), 93. <https://doi.org/10.1609/aimag.v29i3.2157>
 - [63] Yakun Sophia Shao, Jason Clemons, Rangharajan Venkatesan, Brian Zimmer, Matthew Fojtik, Nan Jiang, Ben Keller, Alicia Klinefelter, Nathaniel Pinckney, Priyanka Raina, Stephen G. Tell, Yanqing Zhang, William J. Dally, Joel Emer, C. Thomas Gray, Bruce Khailany, and Stephen W. Keckler. 2019. Simba: Scaling deep-learning inference with multi-chip-module-based architecture. In *MICRO*. 14–27.
 - [64] Franyell Silfa, Gem Dot, Jose-Maria Arnau, and Antonio Gonazález. 2019. Neuron-Level Fuzzy Memoization in RNNs. In *MICRO*.
 - [65] Kevin Siu, Dylan Malone Stuart, Mostafa Mahmoud, and Andreas Moshovos. 2018. Memory Requirements for Convolutional Neural Network Hardware Accelerators. In *IISWC*.
 - [66] Nitish Srivastava, Hanchen Jin, Shaden Smith, Hongbo Rong, David Albonesi, and Zhiru Zhang. 2020. Tensaurus: A Versatile Accelerator for Mixed Sparse-Dense Tensor Computations. In *HPCA*.
 - [67] Lubos Takac and Michal Zabovsky. 2012. Data analysis in public social networks. In *DTI*.
 - [68] Rajeev Thakur, Rolf Rabenseifner, and William Gropp. 2005. Optimization of Collective Communication Operations in MPICH. *IJHPCA* (2005).
 - [69] Shyamkumar Thoziyoor, Naveen Muralimanohar, Jung Ho Ahn, and Norman P Jouppi. 2008. *CACTI 5.1*. Technical Report. 2008-20, HP Labs.
 - [70] Shikhar Vashishth. 2019. Neural graph embedding methods for natural language processing. *arXiv preprint* (2019).
 - [71] Kuansan Wang, Zhihong Shen, Chiyuan Huang, Chieh-Han Wu, Yuxiao Dong, and Anshul Kanakia. 2020. Microsoft academic graph: When experts are not enough. *Quantitative Science Studies* 1, 1 (2020), 396–413.
 - [72] Yang Wang, Chen Zhang, Zhiqiang Xie, Cong Guo, Yunxin Liu, and Jingwen Leng. 2021. Dual-side Sparse Tensor Core. In *ISCA*.
 - [73] Xuechao Wei, Yun Liang, and Jason Cong. 2019. Overcoming Data Transfer Bottlenecks in FPGA-based DNN Accelerators via Layer Conscious Memory Management. In *DAC*.
 - [74] Keyulu Xu, Weihua Hu, Jure Leskovec, and Stefanie Jegelka. 2018. How powerful are graph neural networks? *arXiv preprint* (2018).
 - [75] Mingyu Yan, Lei Deng, Xing Hu, Ling Liang, Yujing Feng, Xiaochun Ye, Zhimin Zhang, Dongrui Fan, and Yuan Xie. 2020. HyGCN: A gcn accelerator with hybrid architecture. In *HPCA*.
 - [76] Pinar Yanardag and SVN Vishwanathan. 2015. Deep graph kernels. In *KDD*.
 - [77] Jaewon Yang and Jure Leskovec. 2015. Defining and evaluating network communities based on ground-truth. *Knowledge and Information Systems* 42, 1 (2015), 181–213.
 - [78] Xuan Yang, Mingyu Gao, Jing Pu, Ankita Nayak, Qiaoyi Liu, Steven Emberton Bell, Jeff Ou Setter, Kaidi Cao, Heonjae Ha, Christos Kozyrakis, and Mark Horowitz. 2018. DNN dataflow choice is overrated. *arXiv preprint* (2018).
 - [79] Yifan Yang, J. Emer, and Daniel Sánchez. 2021. SpZip: Architectural Support for Effective Data Compression In Irregular Applications. In *ISCA*.
 - [80] Pengcheng Yao, Long Zheng, Zhen Zeng, Yu Huang, Chuangyi Gui, Xiaofei Liao, Hai Jin, and Jingling Xue. 2020. A locality-aware energy-efficient accelerator for graph mining applications. In *MICRO*.
 - [81] Muhan Zhang and Yixin Chen. 2018. Link prediction based on graph neural networks. In *NeurIPS*.
 - [82] Mingxing Zhang, Youwei Zhuo, Chao Wang, Mingyu Gao, Yongwei Wu, Kang Chen, Christos Kozyrakis, and Xuehai Qian. 2018. GraphP: Reducing communication for PIM-based graph processing with efficient data partition. In *HPCA*.
 - [83] Shijin Zhang, Zidong Du, Lei Zhang, Huiyang Lan, Shaoli Liu, Ling Li, Qi Guo, Tianshi Chen, and Yunji Chen. 2016. Cambricon-X: An Accelerator for Sparse Neural Networks. In *MICRO*.
 - [84] Xi Zhang, Chongmin Li, Haixia Wang, and Dongsheng Wang. 2010. A Cache Replacement Policy Using Adaptive Insertion and Re-reference Prediction. In *2010 22nd International Symposium on Computer Architecture and High Performance Computing*. 95–102. <https://doi.org/10.1109/SBAC-PAD.2010.21>
 - [85] Zhekai Zhang, Hanrui Wang, Song Han, and William J. Dally. 2020. SpArch: Efficient Architecture for Sparse Matrix Multiplication. In *HPCA*.
 - [86] Da Zheng, Disa Mhembere, Vince Lyzinski, Joshua T Vogelstein, Carey E Priebe, and Randal Burns. 2016. Semi-external memory sparse matrix multiplication for billion-node graphs. *TPDS* (2016).
 - [87] Xuda Zhou, Zidong Du, Qi Guo, Shaoli Liu, Chengsi Liu, Chao Wang, Xuehai Zhou, Ling Li, Tianshi Chen, and Yunji Chen. 2018. Cambricon-S: Addressing Irregularity in Sparse Neural Networks through a Cooperative Software/Hardware Approach. In *MICRO*.
 - [88] Maohua Zhu, Tao Zhang, Zhenyu Gu, and Yuan Xie. 2019. Sparse Tensor Core: Algorithm and Hardware Co-Design for Vector-wise Sparse Neural Networks on Modern GPUs. In *MICRO*.
 - [89] Xiaowei Zhu, Wentao Han, and Wenguang Chen. 2015. GridGraph: Large-scale graph processing on a single machine using 2-level hierarchical partitioning. In *ATC*.
 - [90] Youwei Zhuo, Chao Wang, Mingxing Zhang, Rui Wang, Dimin Niu, Yanzhi Wang, and Xuehai Qian. 2019. GraphQ: Scalable PIM-based graph processing. In *MICRO*.